Desalination and Water Treatment
www.deswater.com
doi: 10.5004/dwt.2021.26811

211 (2021) 359–368
January

Improving the reverse osmosis desalination system with tilted oval spacers in a zigzag configuration

Mounir Amokrane[a,b,*], Djamel Sadaoui[a]

[a]*Faculté de Technologie, Laboratoire de Mécanique Matériaux et Energétique (L2ME), Université de Bejaia, Bejaia, Algérie, Tel. +21365856919; email: mounir139@live.fr (M. Amokrane), Tel. +213559826301; email: sadaouidjamel@yahoo.fr (D. Sadaoui)*
[b]*Département de Génie Mécanique, Faculté du Génie de la Construction, Université Mouloud Mammeri de Tizi Ouzou, Tizi Ouzou, Algérie*

Received 29 April 2020; Accepted 16 November 2020

ABSTRACT

Seawater reverse osmosis desalination is an efficient way to produce pure water from seawater, however, its cost remains high, which motivates us to make some improvements in the process, such as the design for more efficient membrane modules. Given this, a two-dimensional CFD model is used to carry out a comparative study between commercial feed spacers arranged in a zigzag configuration and novel designs of feed spacers, that is, oval tilted spacers. In comparison to the models most reported in the literature, the unit cell approach used in this modeling appears to be more representative of the complete membrane module and needs less computational resources. The numerical simulations performed for inlet mass fractions ranging from 0.0002 to 0.002 kg/kg and transmembrane pressures ranging from 81 to 1,247 kPa show that cells equipped with 20° tilted ovals generate ~ 2% less salt deposition on the membranes and produce ~ 1% more permeate flux than the commercial design. These encouraging results quantified for a single cell are expected to increase for a complete membrane module composed of thousands of cells.

Keywords: Concentration polarization; CFD; Desalination; New spacer designs

1. Introduction

Reverse osmosis is the most used membrane process to desalinate sea and brackish waters. It consists of applying a pressure greater than the osmotic pressure of the salt-water through a semipermeable membrane, thus generating a pure water flux. The modeling of fluid mechanics phenomena occurring in the membrane systems have been widely discussed in the literature [1–3], either in empty channels [4–12], channels fitted with square-shaped spacers [13–17], or commercial configurations [18–28]. In that regard, Cao et al. [18] investigated the effects of various arrangements of turbulence promoters. Their simulation results showed that circular spacers improve the local shear stress on the membrane surface and produce eddy activities that enhance the mass transfer. Schwinge et al. [19–22] studied the flow field and concentration distribution for different configurations (submerged, cavity, and zigzag), and geometric parameters were optimized to achieve better performances. Koutsou et al. [23] simulated the two-dimensional flow in narrow channels with transverse turbulence promoters to better understand the fluid flow behavior. Later, they expanded their simulations to more realistic configurations [24]. Subramani et al. [25] carried out simulations to assess pressure, flow, and concentration profiles in open and spacer-filled cross-flow channels. They concluded that the zigzag spacer configuration might promote fouling and scaling; while the cavity and submerged configurations appear better suited to promote the mass transfer. Wardeh and Morvan [26] studied the role of spacers in the feed channel to increase

* Corresponding author.

Presented at the International Conference on Sustainable Water Treatment Technologies and Environment (SUST-WATER 2019), 14–16 October 2019, Tipasa, Algeria

shear stress, cleaning the precipitated salt accumulated on the membrane surface. Their conclusions suggest that the zigzagging type spacers are more economical and more efficient in removing accumulated salt from the membrane surface compared to the submerged one. Sousa et al. [27] carried out CFD simulations in 2D membrane feed channel models by varying the inter-filament distance and flow velocity. Their results revealed that the inter-filament distance had a significant impact on the velocity field, the local and average friction factors, the pressure drop, and the shear stress on the membrane walls. Amokrane et al. [28] have dealt with the spatial development and the evolution of concentration polarization distribution in spacer-filled channels by taking into account the time-varying behavior of the flow field in these systems. Zigzag and submerged configurations were studied and their performances were compared. The results suggested that the zigzag configuration admits better performance compared to the submerged configuration but may accelerate the fouling.

The literature reports some contributions aimed to develop novel spacer designs [29–35]. Thus, Li et al. [29] focused on the development of novel feed spacers that could generate a higher mass transfer than non-woven spacers. They concluded that the optimal flow pattern in spacer-filled channels is characterized by the co-existence of transverse and longitudinal vortices. Dendukuri et al. [30] reported in their paper a CFD simulation for spacers with non-circular filament cross-sections. Four new designs were proposed and evaluated. They showed that certain new spacer filaments designs could improve the performances by reducing the pressure drop across spacer-filled channels. Ahmad et al. [31,32] studied the impact of basic forms as circular, square, and triangular on flow patterns and mass transfer. They noticed that for usual flow velocities, cylindrical spacers generate lower concentration factor compared to rectangular spacers. While, for high flow velocities, triangular filaments admit the best compromise between concentration polarization and pressure drop, followed by square and circular filaments. Ranade and Kumar [33] considered the effects of new spacer shapes on fluid dynamics and noticed that some novel spacers affect the fluid flow behavior and may reduce the pressure drop. Guillen and Hoek [34] investigated the impact of new spacer designs (square, ellipse, and wing) on mass transfer, pressure drop, water quality, and energy consumption. Their results indicate that at low operating pressure, certain newly designed spacers might minimize hydraulic losses. Amokrane et al. [35] compared desalination performances of channels filled by numerous oval, elliptic and rounded filaments and found a higher pressure drop in systems with circular filaments. Also, oval and elliptic cross-sections might have a better ability to reduce concentration polarization layer thickness.

The literature survey shown above reveals that most computational investigations suggest the modeling of the membrane system as a feed channel filled with a limited number of spacers (e.g., [19–22,28,29,34,35]). This approach requires important computational resources and does not accurately reflect an entire membrane module comprising thousands of spacers. In this work, it is proposed to model a unit cell of a membrane module, which leads to a significant reduction of the computation time and represents better the entire membrane system. Thus, a two-dimensional unit cell model is used to perform a broad comparison between the commercial zigzag configuration and oval tilted spacer designs in respect to the concentration polarization control, pure water production, and power consumption handling at various feed solution concentrations and transmembrane pressures.

2. Modeling

2.1. Spacer geometries

Fig. 1 shows the 3D schematic representations of the designed unit cells to be evaluated in this study, where the physical domains of interest are 2-dimensional cross-sections of 16 mm length (L) and 2 mm height (H). Spacers have similar cross-sections and are 8 mm apart [35]. The oval spacers are tilted at various angles (ϕ) relative to the horizontal axis and are named according to their inclination, as follows: oval ($\phi = 0°$), oval ($\phi = 10°$), and oval ($\phi = 20°$).

2.2. Governing equations, fluid properties and boundary conditions

The numerical model for fluid flow and mass transfer within the physical domains was developed under some assumptions as steady, isothermal, laminar, and incompressible Newtonian fluid. Further, gravity, viscous dissipation, and compressibility effects are neglected. Under these assumptions, the equations of continuity, momentum, and mass transfer are written as follows:

Continuity equation:

$$\frac{\partial(\rho u)}{\partial x}+\frac{\partial(\rho v)}{\partial y}=0 \tag{1}$$

Momentum equations:

$$u\frac{\partial(\rho u)}{\partial x}+v\frac{\partial(\rho u)}{\partial y}=-\frac{\partial p}{\partial x}+\frac{\partial}{\partial x}\left(\mu\frac{\partial u}{\partial x}\right)+\frac{\partial}{\partial y}\left(\mu\frac{\partial u}{\partial y}\right) \tag{2}$$

$$u\frac{\partial(\rho v)}{\partial x}+v\frac{\partial(\rho v)}{\partial y}=-\frac{\partial p}{\partial y}+\frac{\partial}{\partial x}\left(\mu\frac{\partial v}{\partial x}\right)+\frac{\partial}{\partial y}\left(\mu\frac{\partial v}{\partial y}\right) \tag{3}$$

Solute equation:

$$\frac{\partial(\rho u m_A)}{\partial x}+\frac{\partial(\rho v m_A)}{\partial y}=\frac{\partial}{\partial x}\left(\rho D_{AB}\frac{\partial m_A}{\partial x}\right)+\frac{\partial}{\partial y}\left(\rho D_{AB}\frac{\partial m_A}{\partial y}\right) \tag{4}$$

In the above equations, ρ, μ, u, v, and p represent respectively the density, dynamic viscosity, x velocity, y velocity, and pressure, while m_A and D_{AB} are the salt mass fraction and the binary diffusion coefficient of the solute A in the solvent B, respectively.

The numerical model considers that a mixture of pure water and sodium chloride flows inside the cells shown in Fig. 1. The physicochemical properties of the mixture defined

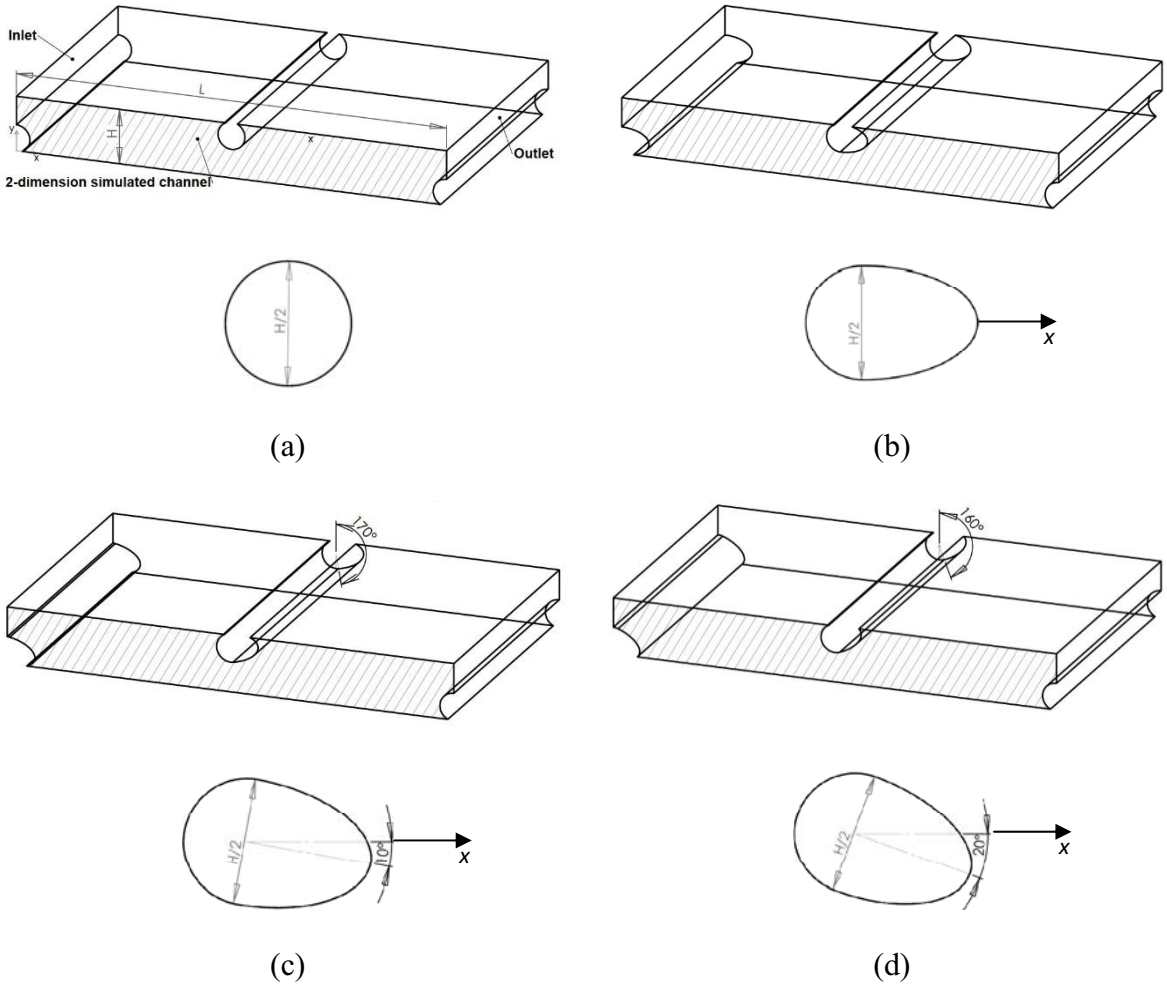

Fig. 1. Schematic representations of the modeled unit cells: (a) circular spacer, (b) oval spacer (ϕ = 0°), (c) oval spacer (ϕ = 10°), and (d) oval spacer (ϕ = 20°).

in Eqs. (5)–(8) depend on the salt mass fraction and are valid for $m_A \le 0.09$ kg/kg [4].

$$\pi = 805.1 \times 10^5 m_A \tag{5}$$

$$\mu = 0.89 \times 10^{-3}\left(1 + 1.63 m_A\right) \tag{6}$$

$$D_{AB} = \max\left(1.61 \times 10^{-9}\left(1 - 14 m_A\right), 1.45 \times 10^{-9}\right) \tag{7}$$

$$\rho = 997.1 \times \left(1.0 + 0.696 m_A\right) \tag{8}$$

In the last equations, π is the transmembrane pressure, while μ, D_{AB}, and ρ are respectively the viscosity, the binary diffusion coefficient and the density of the aqueous solution.

Given the geometry repetitiveness within a membrane module, it is expected that the flow pattern has a periodically repeating nature. To represent this quasi-periodicity, inlet velocity profiles (u_0) obtained from previous simulations using a periodic boundary condition are applied at the entrances of each cell, while an outflow boundary condition is applied at the outlets. Meanwhile, the inlet mass fraction (m_{A0}) varies between 0.0002 and 0.007 kg/kg, and no-slip velocity and no solute flux are assumed on the surfaces of the spacers. Profiles of the inlet velocity (u_0) are shown in Fig. 2.

The upper and lower membranes are supposed impermeable to the salt (R = 0.99) and have a constant membrane resistance (R_m = 1.562 × 1,014 m^{-1}). The applied pressure (ΔP_{tm}) across the sides of the membranes varies between 8.103 × 10^5 Pa and 12.47 × 10^5 Pa [36]. Concentration polarization and permeation flux are coupled on the membranes according to Eq. (9).

$$\left.\begin{aligned} u &= 0 \\ v = \pm J_v &= \pm \frac{1}{R_m \mu_w}\left(\Delta P_{tm} - \Delta\pi\right) \\ J_v \cdot R \cdot m_A &= -D_{AB}\frac{\partial m_A}{\partial y} \end{aligned}\right\} \tag{9}$$

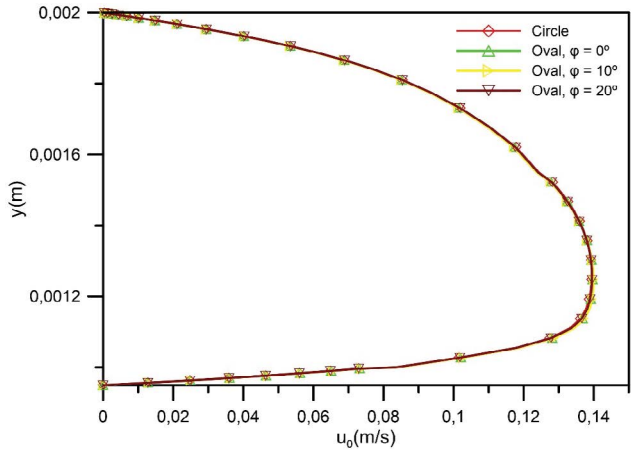

Fig. 2. Inlet velocity profiles (u_0) applied at each unit cell (Re_{ch} = 240).

The positive sign (+) indicates the upper membrane, while the negative (–) represents the lower membrane.

In Eq. (9), μ_w is the dynamic viscosity of the pure water, J_v is the permeate flux, ΔP_{tm} is the transmembrane pressure across the membranes, and $\Delta\pi$ is the osmotic pressure difference between the sides of the membranes.

Concentration polarization due to the accumulation of the rejected solutes on the membranes promotes the formation of a polarized layer. According to the film theory [28], the thickness of this layer can be estimated using Eq. (10).

$$\delta = \ln\left(\frac{m_{Am}R}{m_{A0}-(1-R)m_{Am}}\right)\times\frac{D_{AB}}{J_v} \tag{10}$$

Therefore, the mass transfer coefficient for an un-fouled membrane is linearly related to the concentration layer thickness by Eq. (11), while the Sherwood number is calculated using Eq. (12).

$$k = \frac{D_{AB}}{\delta} \tag{11}$$

$$Sh_{ch} = \frac{kH}{D_{AB}} \tag{12}$$

The power number defined in Eq. (13) is another parameter to estimate the energy consumption of the modeled cells; it is widely used in the literature as a performance parameter [29].

$$Pn = \bar{f}\,Re_{ch}^3 \tag{13}$$

where $\bar{f}$ and Re_{ch}, the average friction factor along with spacer geometries and the Reynolds number defined in Eqs. (14) and (15), respectively:

$$\bar{f} = \frac{H\Delta p}{L\rho u_0^2} = \frac{12}{Re_{ch}} \tag{14}$$

$$Re_{ch} = \frac{\rho u_0 H}{\mu} \tag{15}$$

2.3. Numerical procedure

The governing equations (continuity, momentum, and mass transfer) with the prescribed boundary conditions are solved numerically by the finite volume method under the non-uniform grid system in x and y directions [37]. The defined solver uses a pressure correction based on an iterative SIMPLE algorithm and the convective terms are discretized using the second-order upwind scheme. To check the convergence of the sequential iterative solution, the normalized residual is calculated for the mass, momentum, and mass transfer equations. Convergence is therefore reached when the residual factor is less than 10^{-8}. The computational grid size contains 11,896 nodes for the cells fitted with circular and non-tilted oval spacers and 12,026 nodes for the cells fitted with ovals inclined at 10° and 20°. Moreover, the mesh is refined near the membrane surfaces to accurately estimate the concentration polarization boundary layer [28].

2.4. Validity of the unit cell approach

The validity of the unit cell approach is performed by comparing the simulation results of the commercial cell (Fig. 1a) with those of Amokrane et al. [28] and [35]. Figs. 3a and b compare the average values of δ, k, and Sherwood number obtained by the current model with those obtained in Amokrane et al. [28] and [35], respectively. The simulations results agree well, with a slight disparity probably due to the applied conditions.

3. Results and discussion

First, the unit cells shown in Fig. 1 are evaluated to generate the friction between Re_{ch} = 100 and 380 ($u_0 \approx 0.0442$ and 0.169 m/s). Fig. 4 reveals that the non-tilted oval spacer (ϕ = 0°) generates the highest friction factor compared to the other spacer shapes. This is largely due to the brutal changes in the flow field and the induced pressure drop, while the circular and oval spacers (ϕ = 10° and ϕ = 20°) produce comparable friction. It is worthy to note the good agreement between our numerical estimation of the average friction factor and the theoretical values given by Eq. (14) [27].

The space-averaged values of the salt mass fraction ($\overline{m_{Am}}$) and permeate flux ($\overline{J_v}$) recorded on the membrane walls are plotted against the pressure drop gradient (Δp/L) in Figs. 5 and 6, respectively.

Fig. 5 shows the same trend on both upper and lower membranes, where the cell fitted with oval spacers (ϕ = 20°) generates lower salt deposition on membranes than the other cells at the same axial pressure drop gradient. In other words, it achieves the best deal between the membrane cleaning and the energy consumption compared to the other designs. Indeed, this spacer shape is known to minimize the salt deposition on membranes and causes a lower axial pressure drop than the other spacer shapes [35]. Cells fitted with circular or oval spacers (ϕ = 10°) tend to

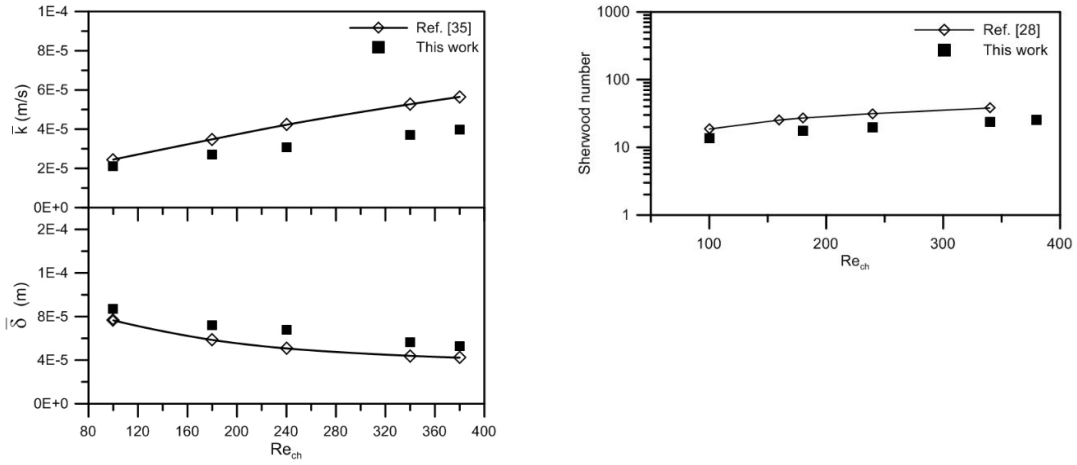

Fig. 3. Comparison with the literature results: (a) the mass transfer coefficient and the thickness of the CP layer and (b) Sherwood number.

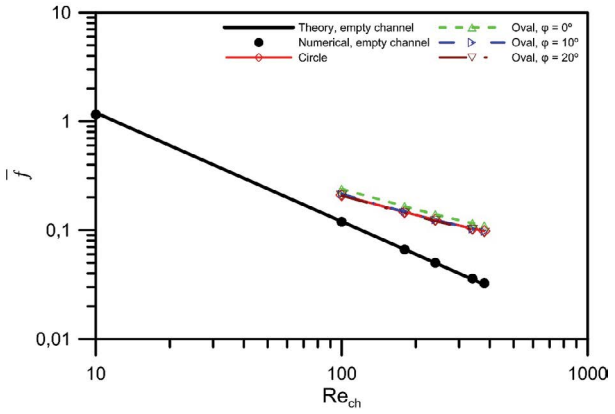

Fig. 4. Average friction factor for an empty channel and the unit cells (Re$_{ch}$ = 100–380).

have similar performance, whereas the cell fitted with oval spacers (ϕ = 0°) generates the poorest performance.

Fig. 6 shows the good performances of the cell fitted with oval spacers (ϕ = 20°) that produces a higher permeate flux compared to the other designs subjected to the same axial pressure drop gradient. It is important to note that cells fitted with circular or inclined oval spacers (ϕ = 10°) record a close performance on the lower membrane, while the circular spacers produce a higher permeate flux than the oval spacers (ϕ = 10°) on the upper membrane.

Fig. 7 shows the Sherwood number recorded on both membranes according to the power number (Pn). In this regard, for a fixed Pn, the cell with the highest Sherwood number is considered to be the most effective [1]. The same tendency is reported on each membrane wall, where the cell fitted with non-tilted oval spacers (ϕ = 0°) records the poorest performance, while the other designs

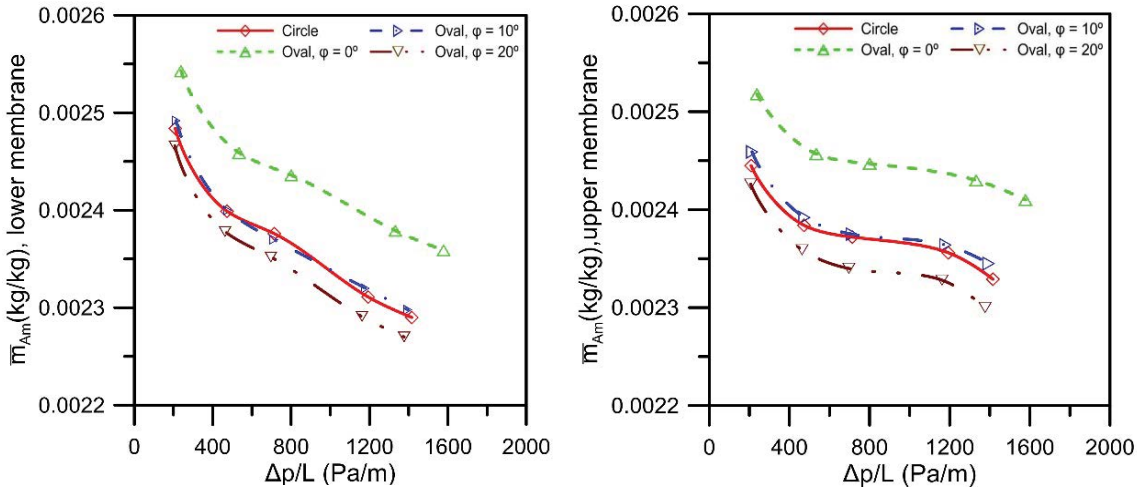

Fig. 5. Space-averaged salt mass fraction as a function of the pressure drop gradient on the lower (a) and the upper (b) membranes (m_{A0} = 0.002 kg/kg and ΔP_{tm} = 81 kPa).

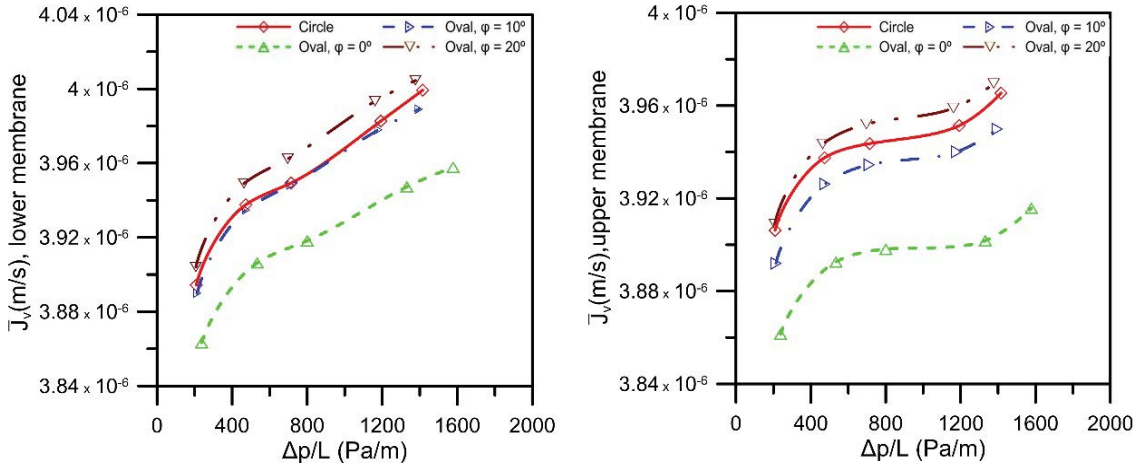

Fig. 6. Space-averaged permeate flux as a function of the pressure drop gradient on the lower (a) and the upper (b) membranes (m_{A0} = 0.002 kg/kg and ΔP_{tm} = 81 kPa).

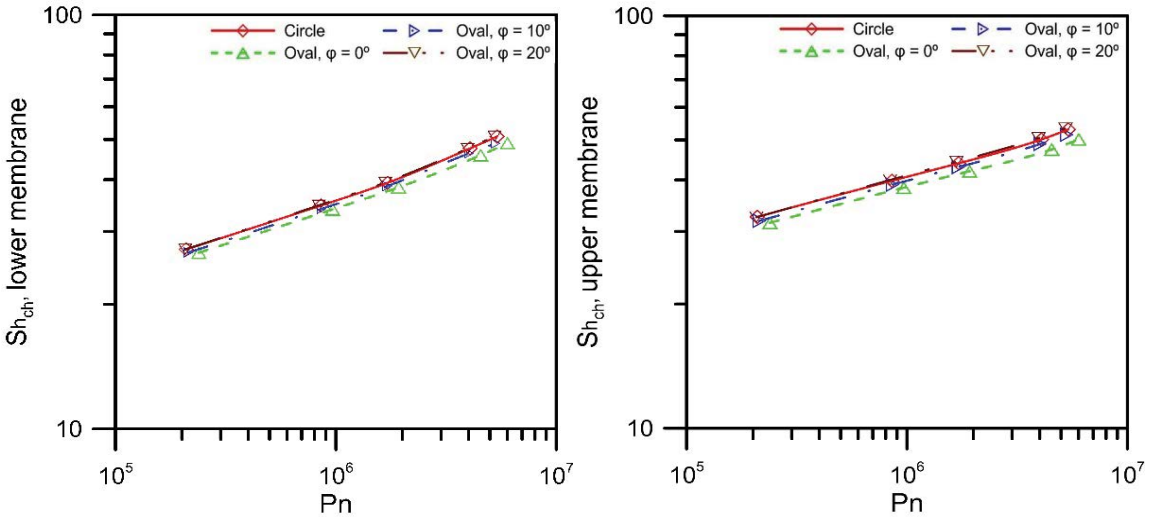

Fig. 7. Sherwood number vs. power number on the lower (a) and the upper (b) membranes (m_{A0} = 0.002 kg/kg and ΔP_{tm} = 81 kPa).

have close performances. Such findings agree with the earlier conclusions of Amokrane et al. [35].

3.1. Performance of unit cells at various salinities of the NaCl solution

This section assesses the desalination efficiency of the unit cells as a function of the feed solution salinity. Inlet mass fractions ranging from 0.0002 to 0.007 kg/kg [5] are tested, while the Reynolds number and the transmembrane pressure are set constants at Re_{ch} = 340 ($u_0 \approx$ 0.1513 m/s) and ΔP_{tm} = 81 kPa, respectively.

Fig. 8 compares the salt mass fraction contours obtained at various m_{A0} of the cells fitted with circular and inclined oval spacers (ϕ = 20°). In both cases, the mass transfer distribution is almost similar [35]; however, regardless the salinity of the feed solution, the salt accumulation observed in the vicinity of the downstream contact points (membranes/spacers) is more important in the commercial cells than in oval spacers designs (ϕ = 20°).

$\overline{m_{Am}}$ and $\overline{J_v}$ recorded on the lower membranes surfaces at different inlet mass fractions for a constant Re_{ch} and ΔP_{tm} are shown in Fig. 9. As expected, increasing the feed solution salinity decreases the produced pure water flux. In these simulations, the cell fitted with ovals (ϕ = 20°) records the lowest salt deposition, and therefore the highest permeate flux. Meanwhile, the cells fitted with circular and oval spacers (ϕ = 10°) generate comparable results, with a slight advantage recorded for the circular spacers.

3.2. Performances of unit cells at different transmembrane pressures

This section is devoted to assessing the unit cell performances at various transmembrane pressures. The simulations are performed for ΔP_{tm} ranging from 81 to 1,247 kPa

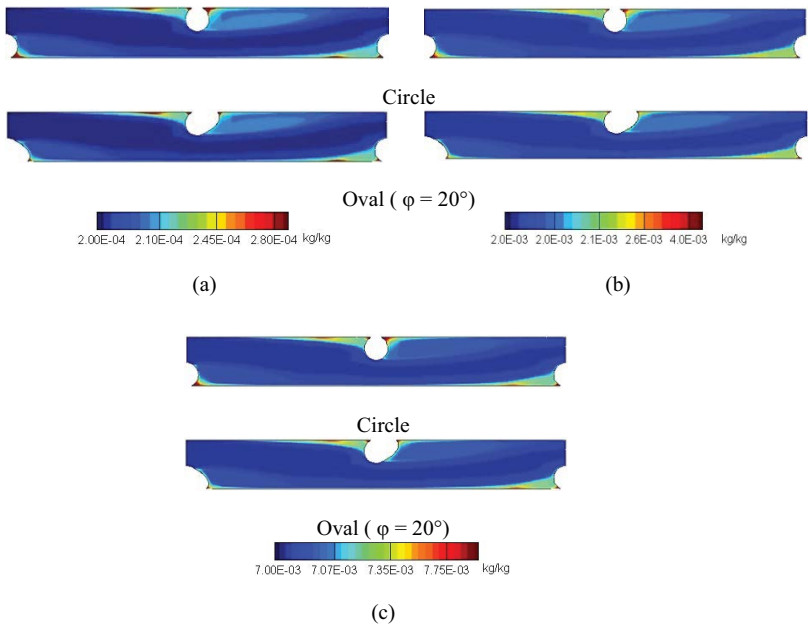

Fig. 8. Contours of the salt mass fraction at various inlet mass fractions: circular and 20° tilted oval spacers (Re_{ch} = 340 and ΔP_{tm} = 81 kPa) (a) m_{A0} = 0.0002 kg/kg, (b) m_{A0} = 0.002 kg/kg, and (c) m_{A0} = 0.007 kg/kg.

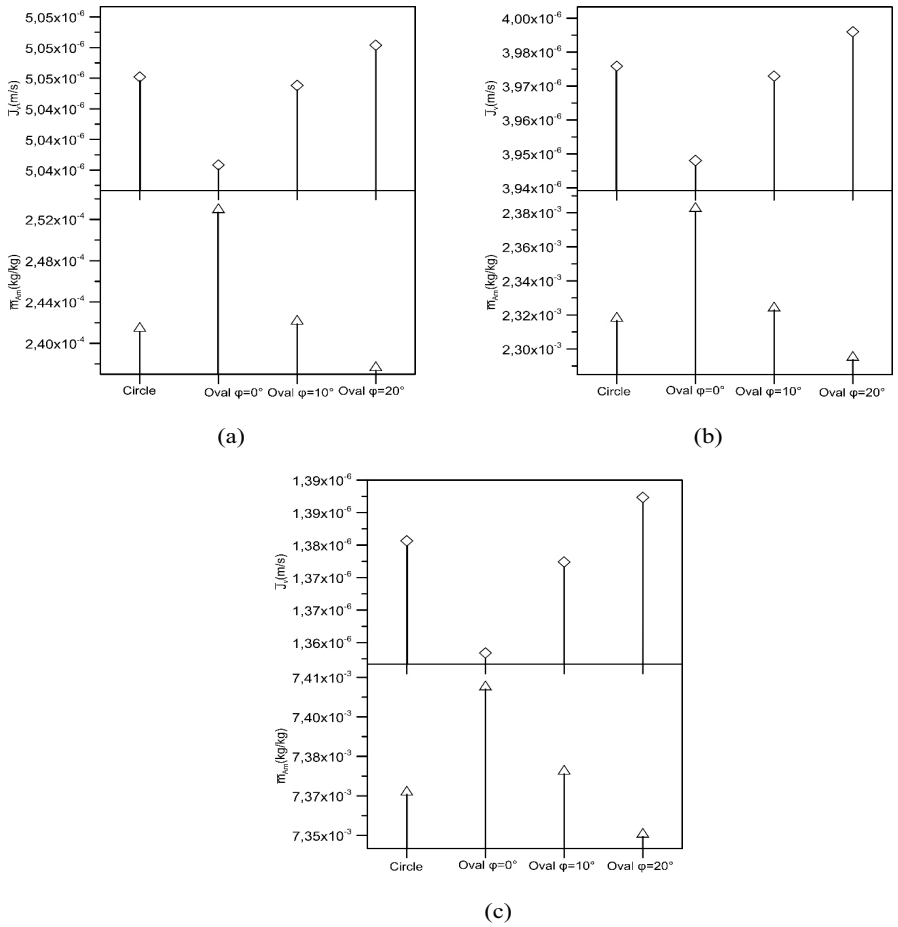

Fig. 9. Space-averaged permeate flux (upper graph) and salt mass fraction (lower graph) recorded on the lower membrane surface at various inlet mass fractions (Re_{ch} = 340 and ΔP_{tm} = 81 kPa) (a) m_{A0} = 0.0002 kg/kg, (b) m_{A0} = 0.002 kg/kg, and (c) m_{A0} = 0.007 kg/kg.

[36] and a constant Reynolds number and inlet mass fraction (Re_{ch} = 340; m_{A0} = 0.002 kg/kg).

Fig. 10 shows the salt mass fraction contours obtained with various ΔP_{tm} for the cell fitted with oval spacers (ϕ = 20°). Increasing ΔP_{tm} leads to an increase of the local salt mass fraction, mainly within recirculations and near the spacers/membranes contact points.

The space-averaged values of m_{am} and J_v recorded on the lower membrane surface at various ΔP_{tm} are shown in Fig. 11, where it is noteworthy that the increase of the transmembrane pressure results in an increase of both the concentration polarization and the permeation flux [5,8]. For all ΔP_{tm} considered in this study, the cell fitted with oval spacers (ϕ = 20°) records the lowest membrane salt deposit and produces the highest permeate flux followed by the commercial cell, then by the cell fitted with oval spacers (ϕ = 10°).

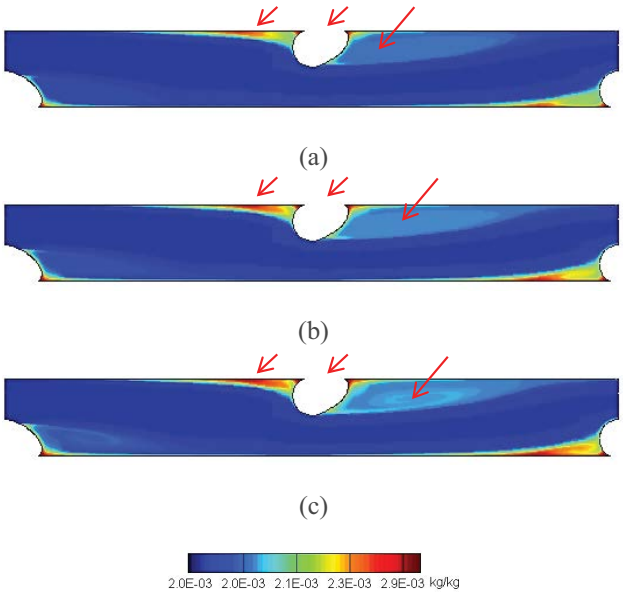

Fig. 10. Contours of the salt mass fraction at various transmembrane pressures for the cell fitted with 20° tilted oval spacers (Re_{ch} = 340 and m_{A0} = 0.002 kg/kg) (a) ΔP_{tm} = 81 kPa, (b) ΔP_{tm} = 1,068.8 kPa, and (c) ΔP_{tm} = 1,247 kPa.

4. Conclusion

This paper describes a numerical investigation of the flow field with mass transfer within a membrane system. The present modeling is based on the unit cell approach, consisting to model a single cell of a membrane module, which significantly reduces the computational resources.

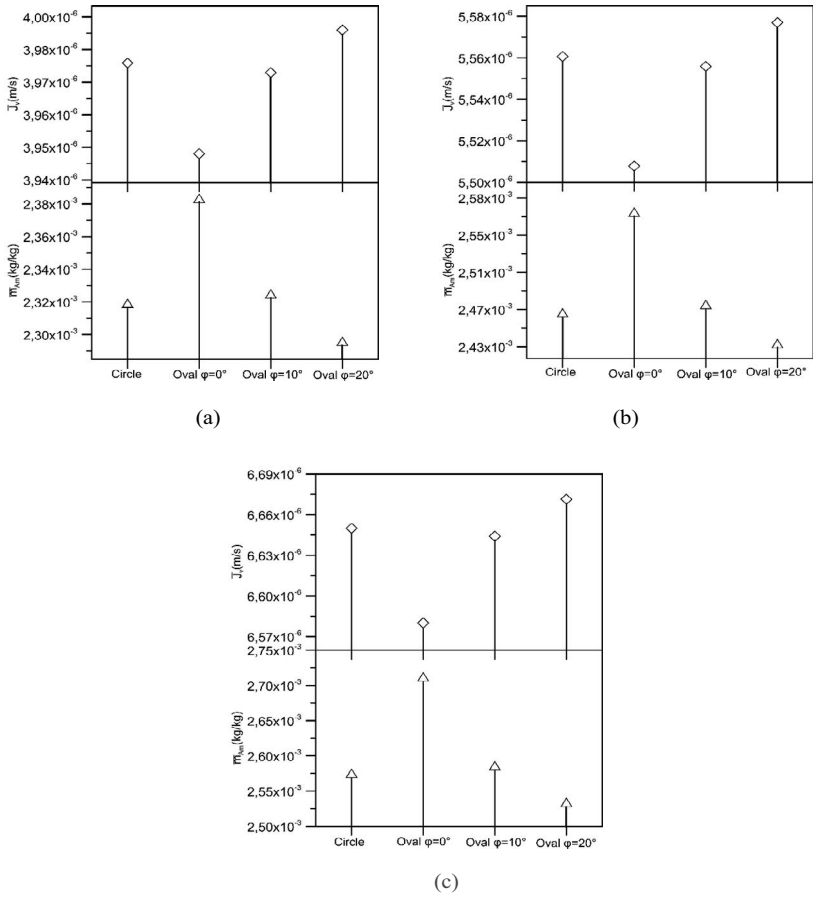

Fig. 11. Space-averaged permeate flux (upper graph) and salt mass fraction (lower graph) recorded on the lower membrane surface at various transmembrane pressures (m_{A0} = 0.002 kg/kg and Re_{ch} = 340) (a) ΔP_{tm} = 81 kPa, (b) ΔP_{tm} = 1,068.8 kPa, and (c) ΔP_{tm} = 1,247 kPa.

The performances of the commercial cell were compared to those of cells fitted with tilted oval spacers in terms of the salt deposition control and pure water production at different salinities of the NaCl solution and various transmembrane pressures.

The numerical results revealed that mounting 20° oval inclined spacers in the membrane channel helps to reduce more efficiently the salt deposit on the surfaces of the membranes which leads to an increase of the permeate flux while limiting the longitudinal pressure losses. Indeed, the cells fitted with 20° inclined ovals recorded better performances than the commercial designs, and this for a wide range of inlet mass fractions ($0.0002 \le m_{A0} \le 0.007$ kg/kg) and transmembrane pressures ($81 \le \Delta P_{tm} \le 1247$ kPa).

Although the tilted oval spacers presented in this study appear to generate better results than the commercial spaces, it is important to note that the production cost of those new designs may be higher than that of the commercial designs, since 3D printing is required.

Symbols

D_{AB} — Binary diffusion coefficient, m²/s
$\bar{f}$ — Friction factor, $H\Delta p/\mathrm{L}\,\rho u_0^2$
H — Unit cell height, m
J_v — Permeation flux, m/s
k — Mass transfer coefficient, (D_{AB}/δ) (m/s)
L — Unit cell length, m
m_A — Salt mass fraction, kg solution/kg solution
p — Pressure, Pa
Pn — Power number, $\bar{f}\ \mathrm{Re}_{ch}^3$
R — Intrinsic rejection coefficient
R_m — Hydraulic resistance of the membrane, m⁻¹
Re_{ch} — Reynolds number based on the unit cell height, $(\rho u_0 H/\mu)$
Sh_{ch} — Sherwood number, kH/D_{AB}
u, v — Velocity components in Cartesian coordinates, m/s
x, y — Cartesian coordinates, m

Greek

δ — Concentration polarization layer thickness, m
ρ — Density, kg/m³
μ — Dynamic viscosity, Pa s
ΔP_{tm} — Transmembrane pressure between the membrane sides, Pa
Δp — Axial pressure drop, Pa
π — Osmotic pressure, Pa
ϕ — Oval spacer inclination, °

Subscripts

0 — Inlet channel
m — Membrane surface
w — Pure water

References

[1] G.A. Fimbres-Weihs, D.E. Wiley, Review of 3D CFD modeling of flow and mass transfer in narrow spacer-filled channels in membrane modules, Chem. Eng. Process. Process Intensif., 49 (2010) 759–781.
[2] A.J. Karabelas, M. Kostoglou, C.P. Koutsou, Modeling of spiral wound membrane desalination modules and plants – review and research priorities, Desalination, 365 (2015) 165–186.
[3] A.H. Haidari, S.G.J. Heijman, W.G.J. van der Meer, Optimal design of spacers in reverse osmosis, Sep. Purif. Technol., 192 (2018) 441–456.
[4] V. Geraldes,V. Semião, M.N. Pinho, Numerical modelling of mass transfer in slits with semi-permeable membrane walls, Eng. Comput., 17 (2000) 192–217.
[5] V. Geraldes, V. Semião, M.N. de Pinho, Flow and mass transfer modelling of nanofiltration, J. Membr. Sci., 191 (2001) 109–128.
[6] M.N. de Pinho, V. Semião, V. Geraldes, Integrated modeling of transport processes in fluid/nanofiltration membrane systems, J. Membr. Sci., 206 (2002) 189–200.
[7] D.E. Wiley, D.F. Fletcher, Techniques for computational fluid dynamics modeling of flow in membrane channels, J. Membr. Sci., 211 (2003) 127–137.
[8] A.L. Ahmad, K.K. Lau, M.Z. Abu Bakar, S.R. Abd. Shukor, Integrated CFD simulation of concentration polarization in narrow membrane channel, Comput. Chem. Eng., 29 (2005) 2087–2095.
[9] S. Kim, E.M.V. Hoek, Modeling concentration polarization in reverse osmosis processes, Desalination, 186 (2005) 111–128.
[10] A. Alexiadis, D.E. Wiley, A. Vishnoi, R.H.K. Lee, D.F. Fletcher, J. Bao, CFD modeling of reverse osmosis membrane flow and validation with experimental results, Desalination, 217 (2007) 242–250.
[11] L.F. Song, C. Liu, A total salt balance model for concentration polarization in crossflow reverse osmosis channels with shear flow, J. Membr. Sci., 401–402 (2012) 313–322.
[12] M. Kostoglou, A.J. Karabelas, Comprehensive simulation of flat-sheet membrane element performance in steady state desalination, Desalination, 316 (2013) 91–102.
[13] V. Geraldes, V. Semião, M.N. de Pinho, Flow management in nanofiltration spiral wound modules with ladder-type spacers, J. Membr. Sci., 203 (2002) 87–102.
[14] V. Geraldes, V. Semião, M.N. de Pinho, The effect of the ladder-type spacers configuration in NF spiral-wound modules on the concentration boundary layers disruption, Desalination, 146 (2002) 187–194.
[15] V. Geraldes, V. Semião, M.N. de Pinho, Hydrodynamics and Concentration polarisation and flow structure within nanofiltration spiral-wound modules with ladder-type spacers, Desalination, 157 (2003) 395–402.
[16] S.W. Ma, L.F. Song, S.L. Ong, W.J. Ng, A 2-D streamline upwind Petrov/Galerkin finite element model for concentration polarization in spiral wound reverse osmosis modules, J. Membr. Sci., 244 (2004) 129–139.
[17] S.W. Ma, L.F. Song, Numerical study on permeate flux enhancement by spacers in a crossflow reverse osmosis channel, J. Membr. Sci., 284 (2006) 102–109.
[18] Z. Cao, D.E. Wiley, A.G. Fane, CFD simulations of net-type turbulence promoters in a narrow channel, J. Membr. Sci., 185 (2001) 157–176.
[19] J. Schwinge, D.E. Wiley, D.F. Fletcher, Simulation of the flow around spacer filaments between narrow channel walls. 1. Hydrodynamics, Ind. Eng. Chem. Res., 41 (2002) 2977–2987.
[20] J. Schwinge, D.E. Wiley, D.F. Fletcher, Simulation of the flow around spacer filaments between channel walls. 2. Mass-transfer enhancement, Ind. Eng. Chem. Res., 41 (2002) 4879–4888.
[21] J. Schwinge, D.E. Wiley, D.F. Fletcher, A CFD study of unsteady flow in narrow spacer-filled channels for spiral-wound membrane modules, Desalination, 146 (2002) 195–201.
[22] J. Schwinge, D.E. Wiley, D.F. Fletcher, Simulation of unsteady flow and vortex shedding for narrow spacer-filled channels, Ind. Eng. Chem. Res., 42 (2003) 4962–4977.
[23] C.P. Koutsou, S.G. Yiantsios, A.J. Karabelas, Numerical simulation of the flow in a plane-channel containing a periodic array of cylindrical turbulence promoters, J. Membr. Sci., 231 (2004) 81–90.

[24] C.P. Koutsou, S.G. Yiantsios, A.J. Karabelas, Direct numerical simulation of flow in spacer-filled channels: Effect of spacer geometrical characteristics, J. Membr. Sci., 291 (2007) 53–69.
[25] A. Subramani, S. Kim, E.M.V. Hoek, Pressure, flow, and concentration profiles in open and spacer-filled membrane channels, J. Membr. Sci., 277 (2006) 7–17.
[26] S. Wardeh, H.P. Morvan, CFD simulations of flow and concentration polarization in spacer-filled channels for application to water desalination, Chem. Eng. Res. Des., 86 (2008) 1107–1116.
[27] P. Sousa, A. Soares, E. Monteiro, A. Rouboa, A CFD study of the hydrodynamics in a desalination membrane filled with spacers, Desalination, 349 (2014) 22–30.
[28] M. Amokrane, D. Sadaoui, C.P. Koutsou, A.J. Karabelas, M. Dudeck, A study of flow field and concentration polarization evolution in membrane channels with two-dimensional spacers during water desalination, J. Membr. Sci., 477 (2015) 139–150.
[29] F. Li, W. Meindersma, A.B. de Haan, T. Reith, Novel spacers for mass transfer enhancement in membrane separations, J. Membr. Sci., 253 (2005) 1–12.
[30] D. Dendukuri, S.K. Karode, A. Kumar, Flow visualization through spacer filled channels by computational fluid dynamics-II: improved feed spacer designs, J. Membr. Sci., 249 (2005) 41–49.
[31] A.L. Ahmad, K.K. Lau, Impact of different spacer filaments geometries on 2D unsteady hydrodynamics and concentration polarization in spiral wound membrane channel, J. Membr. Sci., 262 (2005) 138–152.
[32] A.L. Ahmad, K.K. Lau, M.Z. Abu Bakar, Impact of different spacer filament geometries on concentration polarization control in narrow membrane channel, J. Membr. Sci., 286 (2006) 77–92.
[33] V.V. Ranade, A. Kumar, Fluid dynamics of spacer filled rectangular and curvilinear channels, J. Membr. Sci., 271 (2006) 1–15.
[34] G. Guillen, E.M.V. Hoek, Modeling the impacts of feed spacer geometry on reverse osmosis and nanofiltration processes, Chem. Eng. J., 149 (2009) 221–231.
[35] M. Amokrane, D. Sadaoui, M. Dudeck, C.P. Koutsou, New spacer designs for the performance improvement of the zig-zag spacer configuration in spiral-wound membrane modules, Desal. Water Treat., 57 (2016) 5266–5274.
[36] D.C. Sioutopoulos, S.G. Yiantsios, A.J. Karabelas, Relation between fouling characteristics of RO and UF membranes in experiments with colloidal organic and inorganic species, J. Membr. Sci., 350 (2010) 62–82.
[37] S.V. Patankar, Numerical Heat Transfer and Fluid Flow, McGraw-Hill, New York, 1980.